International Journal of Heat and Mass Transfer 51 (2008) 5144–5153

Contents lists available at ScienceDirect

International Journal of Heat and Mass Transfer

journal homepage: www.elsevier.com/locate/ijhmt

# Assessment of the axisymmetric radiative heat transfer in a cylindrical enclosure with the finite volume method

Man Young Kim *

*Department of Aerospace Engineering, Chonbuk National University, Jeonju, Chonbuk 561-756, Republic of Korea*

ARTICLE INFO

*Article history:*
Received 26 October 2007
Received in revised form 21 March 2008
Available online 13 May 2008

*Keywords:*
Radiative heat transfer
Finite volume method
Axisymmetric coordinate
Mapping process
Directional weight

ABSTRACT

The radiative heat transfer in an axisymmetric enclosure containing an absorbing, emitting, and scattering gray medium is investigated by using the finite volume method (FVM). Especially, formulations with the cylindrical base vectors are introduced and its characteristics is discussed by comparing with other solution methods in the finite volume category. By considering the three-dimensional procedure, the angular redistribution term, which appears in such curvilinear coordinates as axisymmetric and spherically symmetric ones, can be treated efficiently without any artifice usually introduced in the conventional discrete ordinates method (DOM). After a mathematical formulation and corresponding discretization equation for the radiative transfer equation (RTE) are derived, final discretization equation is introduced by using the directional weight, which is the key parameter in the FVM since it represents the inflow or outflow of radiant energy across the control volume faces depending on its sign. The present approach is then validated by comparing the present results with those of previous works. All the results presented in this work show that the present method is accurate and valuable for the analysis of cylindrically axisymmetric radiative heat transfer problems.



## 1. Introduction

For many engineering applications such as boilers, combustors, and rocket propulsion systems, axisymmetric assumption is usually made due to its geometric and theoretical simplicity and, thereby, economic benefits because it physically describes three-dimensional phenomena with two-dimensional procedure. Therefore, substantial efforts are exerted to analyze the axisymmetric problems in the field of radiation as wall as flow and heat transfer including combustion. During the past few decades, numerous methods have been proposed to solve the RTE in the axisymmetric geometry. Among others, the conventional $S_N$ DOM was originated by Carlson and Lathrop [1], and developed and applied to combined heat transfer in axisymmetric geometries by Fiveland [2], Jamaluddin and Smith [3], and Kim and Baek [4]. Recently, the FVM is proposed by Chui et al. [5], and further developed by Moder et al. [6], Kim and Baek [7], and Marthy and Mathur [8]. In these methods, the RTE is solved for a set of discrete directions spanning the range of a $4\pi$-solid angle. The total number of equations solved depends on the degree of angular $S_N$ and control angle approximations, respectively.

As a neutron travels through a curvilinear coordinate systems such as cylindrical or spherical one, the propagating direction is constantly varying, even though the neutron does not physically change its direction. This angular redistribution [9] makes it difficult to handle the angular derivative term appearing in these coordinates. To overcome this phenomena so many numerous treatments are suggested, and here, it can be categorized with 3 methods. The first one is the conventional artifice of Carlson and Lathrop [1] and Lewis and Miller [9], where recursive relation for the coefficients $\alpha^{mn\pm1/2}$ is modeled by examining the divergenceless flow condition. Also, Baek and Kim [10] developed a modified discrete ordinates procedure for the analysis in the axisymmetric coordinate following the above artifice. Here, spatial geometry is discretized following the general two-dimensional treatments. Another procedure for angular redistribution is a mapping devised by Chui et al. [5], where axisymmetric spatial and angular two-dimensional intensity $I(r,z,\theta,\phi)$ is transformed into spatial three-dimensional and angular one-coordinate intensity, i.e. $I(r,\varphi_0,z,\theta,\varphi_\Omega=0)$, where, $\phi$ and $\varphi_\Omega$ are the angular azimuthal angle measured from $r$-axis and $x$-axis, respectively, and $\varphi_0$ is the spatial azimuthal angle measured from $x$-axis. Following this novel practice, Chui et al. [11] analyzed the pulverized coal combustion with thermal radiation and Baek and Kim [12] investigated the rocket plume base heating due to searchlight and plume emissions. Similar approach is proposed by Moder et al. [6] for the analysis of non-axisymmetric radiative transfer in cylindrical enclosures. All the procedures in this category use the cylindrical base vector as angular coordinate and require

* Tel.: +82 63 270 2473; fax: +82 63 270 2472.
*E-mail address:* manykim@chonbuk.ac.kr

0017-9310/$ - see front matter © 2008 Elsevier Ltd. All rights reserved.
doi:10.1016/j.ijheatmasstransfer.2008.03.012

**Nomenclature**

$a_I^{mn}$ coefficient of the discretization equation in direction $m$ and $n$ at nodal point $I$
$C_p$ particle concentration, kg/m$^3$
$D_i^{mn} D_i^{mn}$ directional weight in direction $m$ and $n$ at surface $i$, Eq. (4), $i$ = $n$, $s$, $t$, $b$
$D_i^{mn\pm1/2}$ angular edge directional weight in direction $m$ and $n \pm 1/2$ at surface $i$, Eq. (6), $i$ = $e$, $w$
$E$, $W$, $N$, $S$, $T$, $B$ east, west, north, and south neighbor control volumes of current control volume $P$, respectively, see Fig. 3
$e$, $w$, $n$, $s$, $t$, $b$ east, west, north, and south face of the control volume of $P$, respectively, see Fig. 3
$\vec{e}_r, \vec{e}_{\varphi_0}, \vec{e}_z$ cylindrical $r$-, $\varphi_0$-, and $z$-direction base vectors, respectively
$I$ radiative intensity [W/(m$^2$ sr)]
$I_b$ blackbody radiative intensity, $=\sigma T^4/\pi$ [W/(m$^2$ sr)]
$\vec{n}_i$ outward unit normal vector at face $i$, see Fig. 3
$\vec{n}_w$ unit normal vector at the wall towards the medium
$P$ present control volume
$q$ radiative heat flux [W/m$^2$], Eq. (1)
$\vec{r}$ position vector, $= \vec{e}_r r + \vec{e}_{\varphi_0}\varphi_0 + \vec{e}_z z$
$r_c$, $z_c$ cylinder radius and height, respectively [m]
$S_{nr}$ non-radiative volumetric heat source [W/m$^3$], Eq. (18)
$\vec{s}$ direction vector, $= \vec{e}_r \sin\theta\cos\phi + \vec{e}_{\varphi_0}\sin\theta\sin\phi + \vec{e}_z\cos\theta$
$w^{mn}$ angular weight in the DOM

*Greek Symbols*
$\Delta A$, $\Delta V$ surface area and volume of the control volume, respectively
$\Delta\Omega^{mn}$ discrete control angle [sr]
$\alpha^{mn\pm1/2}$ coefficients of the angular derivative term, Eq. (14)
$\beta$ extinction coefficient, $=\kappa_a+\sigma_s$ for gray gas, $=\kappa_{g,k}+\kappa_p+\sigma_{sp}$
$\varepsilon_w$ wall emissivity
$\phi$, $\varphi_\Omega$ angular azimuthal angles measured from the $x'$- and $r$-axis, respectively, see Fig. 1
$\varphi_0$ spatial azimuthal angle measured from the $x$-axis, see Fig. 1
$\kappa_a$, $\sigma_s$ absorption and scattering coefficients of the gray gas, respectively [m$^{-1}$]
$\kappa_{g,k}$ $k$th band absorption coefficient [m$^{-1}$]
$\kappa_p$, $\sigma_{sp}$ absorption and scattering coefficients of the particle, respectively [m$^{-1}$]
$\mu,\eta,\xi$ direction cosines in the $r$-, $\varphi_0$-, and $z$-directions, respectively
$\theta$ angular polar angle measured from the $z$-axis, see Fig. 4
$\sigma$ Stefan–Boltzmann constant, $=5.67\times10^{-8}$ [W/m$^2$ K$^4$]

*Subscripts*
b blackbody
$E$, $W$, $N$, $S$, $T$, $B$ node points where intensities are located
$e$, $w$, $n$, $s$, $t$, $b$ control volume faces
w wall

*Superscripts*
$m$, $n$ radiation directions
$\pm1/2$ control angle faces

the spatial three-dimensional calculation for axisymmetric radiation. The final treatment is a spatial two-dimensional procedure by Murthy and Mathur [8], Tian and Chiu [13], and Ben Salah et al. [14]. Murthy and Mathur [8] implemented general axisymmetric geometric and angular relations, discussed its merits by comparing with the mapping by Chui et al. [5], and applied it to an unstructured body-fitted mesh system. Tian and Chiu [13] proposed a two-dimensional scheme for axisymmetric RTE with the FVM by considering geometric and angular properties of the axisymmetric situations following the work of Murthy and Mathur [8], and discussed the control angle overlaps occurring at the radial side wall of the cylinder. Recently, Ben Salah et al. [14] investigated the explicit expressions of the recursive relation coefficients appearing in the discretized angular redistribution term by using the directional weights.

In this work, a particular implementation of the axisymmetric FVM is introduced that applies to the problems of radiative heat transfer within cylindrical enclosures. The medium may be absorbing, emitting, and isotropically or anisotropically scattering. The gray gas assumption is implicitly used throughout the present article except for the final example of the mixture of non-gray gas and particle. The contributions of this work include (1) a new discretization scheme for axisymmetric problems in the context of the FVM; (2) a mapping that simplifies the solution of axisymmetric radiative heat transfer problems and, thereby, spatial two-dimensional and angular two-dimensional dependence is maintained while angular redistribution term is treated without any artifice to determine the coefficients; (3) a demonstration of performance for the present method. In the following, mathematical formulation and corresponding discretization equation for RTE are derived by considering the mapping procedure that describes the axisymmetric two-dimensional intensity as spatial three-dimensional one by using the cylindrical base vectors as both spatial and angular coordinates. The present approach is then validated by comparing the present results with an exact solution and the predictions obtained from various methods.

## 2. Mathematical formulation

### 2.1. Radiative transfer equation

For a radiatively active medium in a cylindrical enclosure as shown in Fig. 1, the $r$-directional radiative heat flux is defined as

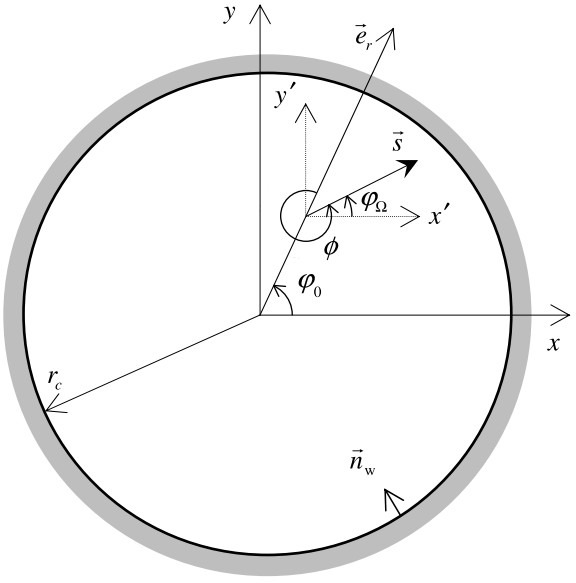


**Fig. 1.** Schematic of the cylindrical enclosure and its coordinate system.

$$q_r^R = \int_{\Omega=4\pi} I(\vec{r},\vec{s})(\vec{s}\cdot\vec{e}_r)\mathrm{d}\Omega \tag{1}$$

where $I(\vec{r},\vec{s})$ is the radiative intensity at position $\vec{r} = \vec{e}_r r + \vec{e}_{\varphi_0}\varphi_0 + \vec{e}_z z$ in the direction $\vec{s} = \vec{e}_r \sin\theta\cos\phi + \vec{e}_{\varphi_0}\sin\theta\sin\phi + \vec{e}_z\cos\theta$, and $\mathrm{d}\Omega = \sin\theta\,\mathrm{d}\theta\,\mathrm{d}\phi$ is the solid angle. The choice of spatial and angular coordinates defining the position and direction is arbitrary. In this study, however, it is noted that the spatial $(r,\varphi_0,z)$ and angular $(\theta,\phi)$ coordinates are selected and defined based on the cylindrical base vectors $\vec{e}_r$, $\vec{e}_{\varphi_0}$, and $\vec{e}_z$. In this case, since the direction of $\vec{e}_r$ and $\vec{e}_{\varphi_0}$ changes as the spatial azimuthal angle $\varphi_0$ changes, the direction $\vec{s}$ defined by a set of $(\theta,\phi)$ changes as $\varphi_0$ changes as shown in Fig. 1. Therefore, it can be found that the angular azimuthal angles, $\phi$ and $\varphi_\Omega$, defined relative to cylindrical and Cartesian coordinates, respectively, are related to the spatial azimuthal angle, $\varphi_0$ through the relation of $\phi = \varphi_\Omega - \varphi_0$.

To obtain the radiative heat flux the radiative intensity at any position, $\vec{r}$, along a path, $\vec{s}$, through an absorbing, emitting, and scattering medium can be evaluated from the following cylindrical RTE [5–7]:

$$\frac{1}{r}\frac{\partial}{\partial r}[\mu r I(\vec{r},\vec{s})] + \frac{1}{r}\frac{\partial}{\partial\varphi_0}[\eta I(\vec{r},\vec{s})] + \frac{\partial}{\partial z}[\xi I(\vec{r},\vec{s})] - \frac{1}{r}\frac{\partial}{\partial\phi}[\eta I(\vec{r},\vec{s})]$$
$$= -\beta(\vec{r})I(\vec{r},\vec{s}) + \kappa_a(\vec{r})I_b(\vec{r}) + \frac{\sigma_s(\vec{r})}{4\pi}\int_{\Omega'=4\pi} I(\vec{r},\vec{s}')\mathrm{d}\Omega' \tag{2}$$

Here, $\mu = \sin\theta\cos\phi$, $\eta = \sin\theta\sin\phi$, and $\xi = \cos\theta$ are the direction cosines of a path, $\vec{s}$, and $\beta(\vec{r}) = \kappa_a(\vec{r}) + \sigma_s(\vec{r})$ is the extinction coefficient of the participating medium, where, $\kappa_a(\vec{r})$ and $\sigma_s(\vec{r})$ are the absorption and scattering coefficients, respectively. Here, it is noted that for the case of axisymmetric situation the $\partial/\partial\varphi_0$ term in Eq. (2) is eliminated, and then, the dependency on spatial three-dimension and angular two-dimension of the intensity $I(r,\varphi_0,z,\theta,\phi)$ is changed to the 2-spatial and 2-angular coordinates, i.e., $I(r,z,\theta,\phi)$. For a diffusely emitting and reflecting wall the above RTE is subject to the following boundary condition:

$$I_w(r_w,\vec{s}) = \varepsilon_w I_b(r_w) + \frac{1-\varepsilon_w}{\pi}\int_{\vec{n}_w\cdot\vec{s}'<0} I(r_w,\vec{s}')|\vec{n}_w\cdot\vec{s}'|\mathrm{d}\Omega' \quad \text{for } \vec{n}_w\cdot\vec{s} > 0 \tag{3}$$

In Eqs. (2) and (3), subscripts b and w denote the black body and bounded wall, respectively. $r_w$ is the radial distance to the bounded wall and $\vec{n}_w$ is the unit normal vector towards medium at the bounding cylindrical wall as shown in Fig. 1.

### 2.2. Finite volume formulations

Our intent is to solve the radiative heat transfer problems using a two-dimensional mesh on the $r-z$ (that is, $\varphi_0 = 0$) plane as shown in Fig. 2a. To formulate the discretization equation describing the axisymmetric behavior, however, three-dimensional control volume shown in Fig. 2b is considered firstly, and then the axisymmetric solution method is discussed. As previously discussed, the axisymmetric radiative heat transfer occurs when the intensity is independent of spatial azimuthal angle $\varphi_0$ and is therefore completely specified by $r$, $z$, $\theta$, and $\phi$. Thereby, the intensity $I(\vec{r},\vec{s})$ is expressed as $I(r,z,\theta,\phi)$. The intensities denoted by $I_2^1$, $I_3^1$, $I_4^1$, and $I_5^1$ shown in Fig. 2b all have the same radius of $r$. The spatial azimuthal angle between all consecutive points is $\pi/4$. The nodal points, 2, 3, 4, and 5 are located at $\varphi_0 = 7\pi/8$, $5\pi/8$, $3\pi/8$, and $\pi/8$, respectively, where $\varphi_0$ is measured from the positive $x$-axis. The angular azimuthal angle measured from Cartesian $x$-axis is $\varphi_\Omega = 0$ for all intensities. Therefore, the angle of $\phi = \varphi_\Omega - \varphi_0$ is $9\pi/8$, $11\pi/8$, $13\pi/8$, and $15\pi/8$ for the intensities $I_2^1$, $I_3^1$, $I_4^1$, and $I_5^1$, respectively. The intensities at point *1* in Fig. 2a all have the same radius of $r$, but are now all located at $\varphi_0 = \pi/2$ with the angular azimuthal angle of $\phi = 15\pi/8$, $13\pi/8$, $11\pi/8$, and $9\pi/8$ for intensities $I_1^5$, $I_1^4$, $I_1^3$, and $I_1^2$, respectively. Thereby it follows that $I_m^1$ and $I_1^m$ have the same value of $r$, $z$, $\theta$, and $\phi$, where $m = 2$, 3, 4, and 5, leading to $I_m^1 = I_1^m$. A simple mapping therefore exists between the intensities in Fig. 2a and b. Here, it is noted that the conventional and modified DOM [2,3,10] calculates intensities $I_1^m$ in Fig. 2a with the cylindrical base vectors to define the angular range, and hence suffers from a directional coupling expressed in terms of angular redistribution. In the FVM by Chui et al. [5], however, the intensities $I_m^1$ in Fig. 2b are computed, and hence, can avoid difficulties in calculating $\propto^{mn\pm1/2}$ terms that arose from the modeling of the angular redistribution. The present procedure is somewhat similar to the work of Chui et al. [5] in view of three-dimensional solution procedure, but they are different in choosing angular coordinates, i.e., $(\theta,\varphi_\Omega)$ in Chui et al. [5] but $(\theta,\phi)$ in the present work. More detailed discussions regarding selection of the angular coordinates are examined in the following.

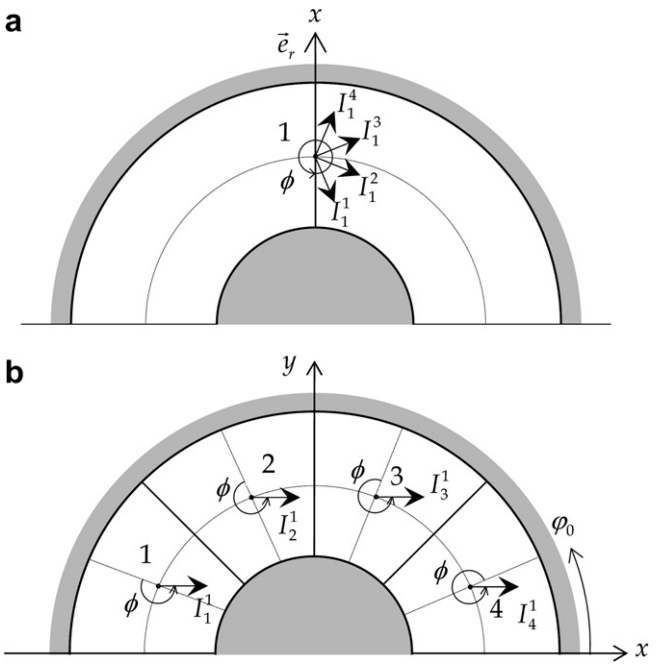


**Fig. 2.** Schematic of the mapping for solution of axisymmetric radiative heat transfer in a cylindrical enclosure: (a) spatial two-dimensional and (b) three-dimensional distributions. Note that $I_k^l$ in (a) is equal to $I_j^k$ in (b).

To explain the finite volume formulations in an axisymmetric enclosure, the first step is to consider the control volume adopted in this method as shown in Fig. 3, which also shows the radiative intensities at each nodal point, *P*, *E*, *W*, *N*, *S*, *T*, and *B* with the unit normal vectors $\vec{n}_i$ at face *i*. The control volume represented by the nodal point, *P*, is enclosed by six control faces denoted by *e*, *w*, *n*, *s*,*t*, and *b*. By using the cylindrical base vectors, $\vec{s} = \vec{e}_r\sin\theta\cos\phi + \vec{e}_{\varphi_0}\sin\theta\sin\phi + \vec{e}_z\cos\theta$, the unit normal vector at each face is expressed as $\vec{n}_i = \vec{e}_r n_{r,i} + \vec{e}_{\varphi_0} n_{\varphi_0,i} + \vec{e}_z n_{z,i}$, so that $\vec{n}_n = -\vec{n}_s = \vec{e}_r$, $\vec{n}_t = -\vec{n}_b = \vec{e}_z$ and $\vec{n}_e = -\vec{n}_w = -\vec{e}_{\varphi_0}$. Fig. 4a shows the polar *m*th and azimuthal *n*th control angle ranging from $\theta^{m-1/2}$ to $\theta^{m+1/2}$ and from $\phi^{n-1/2}$ to $\phi^{n+1/2}$, respectively, which is typically used in the finite volume radiation methods. The angular azimuthal angle measured from the $r$-axis can vary from 0 to $2\pi$. Here, it is noted that the angular azimuthal angle $\phi$ varies for a different $r$-axis as the spatial polar angle, $\varphi_0$, varies as shown in Fig. 3. Thereby, the intensities at point *E* and *W* are represented by $I_E^{m+1}$ and $I_W^{m-1}$, respectively. Similarly, the intensities at face *e* and *w* are expressed by $I_e^{m+1/2}$ and $I_w^{m-1/2}$, respectively. Here, it is explained that the increment of spatial and angular azimuthal angle is chosen to be equal to each other, i.e., $\Delta\varphi_0 = \Delta\phi$. Fig. 4b illustrates the control

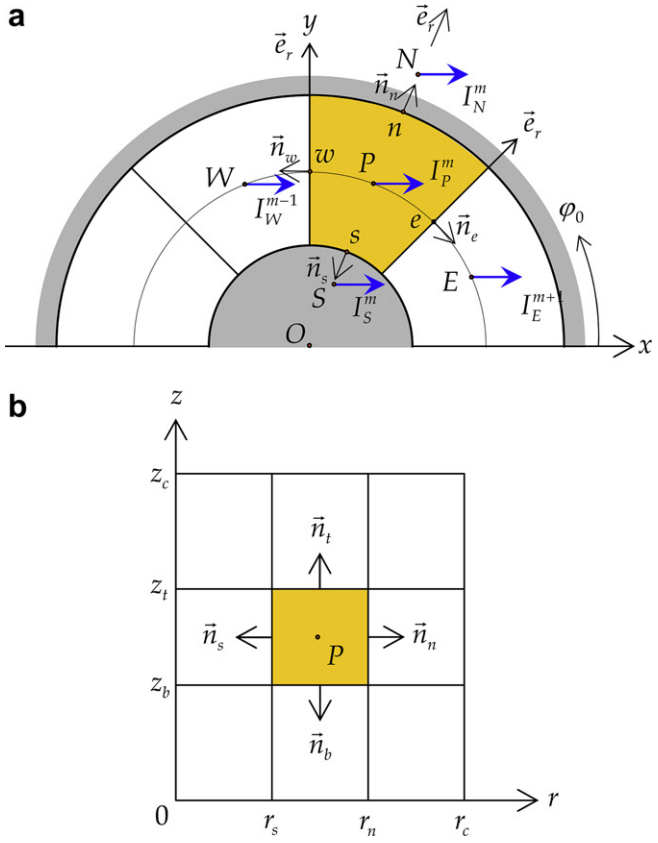


**Fig. 3.** Schematic of a control volume in a cylindrical enclosure with $P$ located at the control volume center: (a) top view and (b) side view.

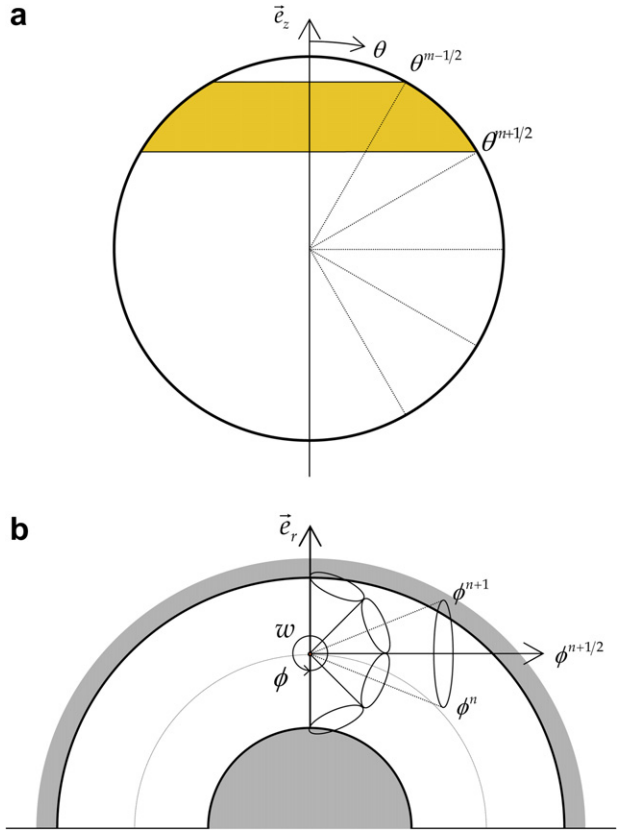


**Fig. 4.** Schematics of the control angle. The angular polar angle $\theta$ in (a) is measured from $z$-axis, while azimuthal angle $\phi$ in (b) is measured from $r$-axis. The polar angle $\theta^m$ is between $\theta^{m-1/2}$ and $\theta^{m+1/2}$. Note that while the azimuthal angle $\phi^n$ ranges from $\phi^{n-1/2}$ to $\phi^{n+1/2}$, the range of angular edge control angle $\phi^{n+1/2}$ is between $\phi^n$ and $\phi^{n+1}$.

angle located at an arbitrary point, for example, face $w$ with total number of control angle of $N_\phi = N_{\varphi_0} = 4$. The $\phi = n + 1/2$th control angle, which is enlarged in Fig. 4b, is an edge control angle ranging from $\phi^n$ to $\phi^{n+1}$.

Attention is now turned to the directional weight at face $i = n$, $s$, $t$, and $b$ through $(m,n)$th control angle, $D_i^{mn}$, to give further explanation for the current solution method. This directional weight, $D_i^{mn}$, denotes the inflow or outflow of radiant energy across the control volume face depending on its sign as defined in the form:

$$D_i^{mn} = \int_{\phi^{n-1/2}}^{\phi^{n+1/2}} \int_{\theta^{m-}}^{\theta^{m+}} (\vec{s}\cdot\vec{n}_i)\sin\theta\,\mathrm{d}\theta\,\mathrm{d}\phi \tag{4}$$

where the unit direction vector, $\vec{s}$, and outward unit normal vector, $\vec{n}_i$, at face $i$ are based on cylindrical coordinates as explained above. Hereafter, $D_i^{mn}$ in each control volume face is discretized as:

$$\begin{aligned} D_n^{mn} = -D_s^{mn} &= \int_{\theta^{m-1/2}}^{\theta^{m+1/2}} \sin^2\theta\,\mathrm{d}\theta \int_{\phi^{n-1/2}}^{\phi^{n+1/2}} \cos\phi\,\mathrm{d}\phi \\ &= \left[\frac{1}{2}(\theta^{m+1/2}-\theta^{m-1/2}) - \frac{1}{4}(\sin 2\theta^{m+1/2} - \sin 2\theta^{m-1/2})\right](\sin\phi^{n+1/2} \\ &\quad - \sin\phi^{n-1/2}) \end{aligned} \tag{5a}$$

$$\begin{aligned} D_t^{mn} = -D_b^{mn} &= \int_{\theta^{m-1/2}}^{\theta^{m+1/2}} \sin\theta\cos\theta\,\mathrm{d}\theta \int_{\phi^{n-1/2}}^{\phi^{n+1/2}} \mathrm{d}\phi \\ &= \frac{1}{2}(\sin^2\theta^{m+1/2} - \sin^2\theta^{m-1/2})(\phi^{n+1/2} - \phi^{n-1/2}) \end{aligned} \tag{5b}$$

Based on this spatial and angular considerations, angular derivative term can be modeled by using the directional weights, which can be obtained through the integration process over a control volume $\Delta V$ and a control angle $\Delta\Omega^{mn}$ such that:

$$\begin{aligned} -\int_{\Delta\Omega}\int_{\Delta V} \frac{1}{r}\frac{\partial}{\partial\phi}(\eta I)\mathrm{d}V\,\mathrm{d}\Omega &\simeq \Delta A_e D_e^{mn+1/2} I_e^{mn+1/2} \\ &\quad + \Delta A_w D_w^{mn-1/2} I_w^{mn-1/2} \end{aligned} \tag{6a}$$

where

$$\begin{aligned} D_e^{mn+1/2} &= -\int_{\theta^{m-1/2}}^{\theta^{m+1/2}} \sin^2\theta\,\mathrm{d}\theta \int_{\phi^n}^{\phi^{n+1}} \sin\phi\,\mathrm{d}\phi \\ &= -\left[\frac{1}{2}(\theta^{m+1/2}-\theta^{m-1/2}) - \frac{1}{4}(\sin 2\theta^{m+1/2} - \sin 2\theta^{m-1/2})\right] \\ &\quad \times (\cos\phi^n - \cos\phi^{n+1}) \end{aligned} \tag{6b}$$

$$\begin{aligned} D_w^{mn-1/2} &= \int_{\theta^{m-1/2}}^{\theta^{m+1/2}} \sin^2\theta\,\mathrm{d}\theta \int_{\phi^{n-1}}^{\phi^n} \sin\phi\,\mathrm{d}\phi \\ &= \left[\frac{1}{2}(\theta^{m+1/2}-\theta^{m-1/2}) - \frac{1}{4}(\sin 2\theta^{m+1/2} - \sin 2\theta^{m-1/2})\right] \\ &\quad \times (\cos\phi^{n-1} - \cos\phi^n) \end{aligned} \tag{6c}$$

are the angular edge directional weights at east and west faces and $\Delta A_e = \Delta A_w = (r_n - r_s)\,\Delta z$ is the surface area of east and west faces, respectively. Here, it is necessary to emphasize that the angular direction $\phi^{n+1/2}$ ranges from $\phi^n$ to $\phi^{n+1}$ as shown in Fig. 4b. It is found that this $\phi^{n+1/2}$ direction is the angular edge where the two control angles meet between $\phi^{n-1/2} < \phi^n < \phi^{n+1/2}$ and $\phi^{(n+1)-1/2} < \phi^{n+1} < \phi^{(n+1)+1/2}$. Therefore, $\Delta A_w D_w^{mn-1/2} I_w^{mn-1/2}$ and $\Delta A_e D_e^{mn+1/2} I_e^{mn+1/2}$ represent the inflow and outflow of the radiant energy through these control faces, i.e., edge control angles, since $D_w^{mn-1/2} < 0$ and $D_e^{mn+1/2} > 0$ are always satisfied regardless of the spatial $\varphi_0$ locations. Fig. 5 illustrates the angular edge directional

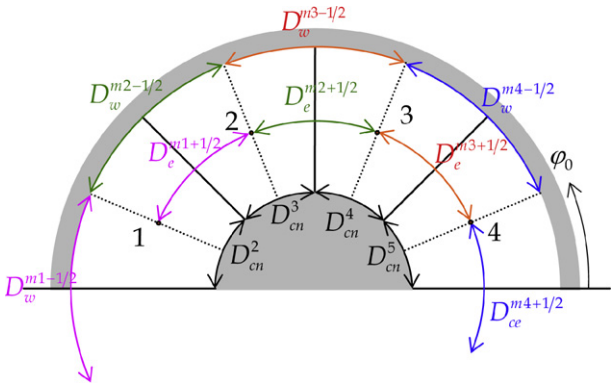


**Fig. 5.** Schematic representation of the directional weights for $N_{\varphi_0} = N_\phi = 4$ case. Note that while the directional weights, $D_n^{mn} = -D_s^{mn}$, covers $n$ and $s$ faces, and the angular edge directional weights, $D_e^{mn+1/2}$ and $D_w^{mn-1/2}$ does $e$ and $w$ faces, respectively.

weights, $D_e^{mn+1/2}$ and $D_w^{mn-1/2}$ with $D_n^{mn} = -D_s^{mn}$. Here, it can be found that $D_e^{mn+1/2} = -D_w^{mn-1/2}$ is satisfied from the geometrical point of view as shown in Fig. 5. Also, it is noted that $D_w^{m1-1/2} = D_e^{mN_\phi+1/2} = 0$ is always satisfied because the azimuthal angular range of $D_w^{m1-1/2}$ and $D_e^{mN_\phi+1/2}$ are perpendicular to the outward unit normal vector at each face, i.e., $\vec{n}_w$ and $\vec{n}_e$. Thereby, the face intensities $I_w^{m1-1/2}$ and $I_e^{mN_\phi+1/2}$ are not necessary to specify for the present computation.

To obtain the finite volume discretized form of the RTE, Eq. (2) is integrated over a control volume, $\Delta V$, and a control angle, $\Delta\Omega^{mn}$, assuming that the magnitude of intensity is constant within $\Delta V$ and $\Delta\Omega^{mn}$, but allowing its direction to vary by following the conventional practice of the FVM [9–11], and then Eq. (6a) is substituted into the integrated form of Eq. (2). Thereby, the following equation can be obtained:

$$\sum_{i=n,s,t,b} I_i^{mn}\Delta A_i D_i^{mn} + [\Delta A_e D_e^{mn+1/2} I_e^{mn+1/2} + \Delta A_w D_w^{mn-1/2} I_w^{mn-1/2}] + \beta I_P^{mn}\Delta V\Delta\Omega^{mn} = S_P^{mn}\Delta V\Delta\Omega^{mn} \tag{7}$$

where $\Delta A_n = r_n\Delta\phi\Delta z$, $\Delta A_s = r_s\Delta\phi\Delta z$, and $\Delta A_t = \Delta A_b = \pi(r_n^2 - r_s^2)/2N_\phi$ are the surface areas of north, south, top, and bottom faces, respectively. $\Delta V = \pi(r_n^2 - r_s^2)\Delta z/2N_\phi$ is the volume of the control volume $P$ and $\Delta\Omega^{mn} = (\cos\theta^{m-1/2} - \cos\theta^{m+1/2})(\phi^{n+1/2} - \phi^{n-1/2})$ is the discrete solid angle.

To relate the facial intensity, $I_i^{mn}$, and the angular edge intensity, $I_i^{mn\pm1/2}$, to the nodal intensity, $I_I^{mn}$, the following simple step scheme popularly used in the DOM and FVM is introduced to ensure positive intensity:

$$I_i^{mn}D_i^m = I_P^{mn}\max(D_i^{mn}, 0) - I_I^{mn}\max(-D_i^{mn}, 0) \tag{8a}$$

$$I_e^{mn+1/2} = I_P^{mn} \tag{8b}$$

$$I_w^{mn-1/2} = I_W^{mn-1} = I_P^{mn-1} \tag{8c}$$

In Eq. (8a), subscript $i$ represents $n$, $s$, $t$ and $b$, while $I$ does the corresponding $N$, $S$, $T$ and $B$. By using this scheme, Eq. (7) can be recast into the following general discretization equation:

$$a_P^{mn} I_P^{mn} = \sum_{I=N,S,T,B} a_I^{mn} I_I^{mn} + b_P^{mn} \tag{9a}$$

where

$$a_P^{mn} = \sum_{i=n,s,t,b} \max(\Delta A_i D_i^{mn}, 0) + \beta\Delta V\Delta\Omega^{mn} + \Delta A_e D_e^{mn+1/2} \tag{9b}$$

$$a_I^m = \max(-\Delta A_i D_i^{mn}, 0) \tag{9c}$$

$$b_P^{mn} = S_P^{mn}\Delta V\Delta\Omega^{mn} - \Delta A_w D_w^{mn-1/2} I_P^{mn-1} \tag{9d}$$

$$S_P^{mn} = \kappa_a I_b + \frac{\sigma_s}{4\pi}\int_{\Omega'=4\pi} I(\vec{r},\vec{s}')d\Omega' \tag{9e}$$

In these formulations the last terms in Eqs. (9b) and (9d) indicate the angular flux of radiant energy, which results from the modeling of angular redistribution term in Eq. (6).

The boundary condition in Eq. (3) for a diffusely reflecting and emitting wall can be arranged to

$$I_w^{mn} = \varepsilon_w I_{b,w} + \frac{1-\varepsilon_w}{\pi}\sum_{m'n',D_w^{m'n'}<0} I_w^{m'n'}|D_w^{m'n'}| \quad \text{for } D_w^{mn} > 0 \tag{10a}$$

where

$$D_w^{mn} = \int_{\Delta\Omega^{mn}} (\vec{s}\cdot\vec{n}_w)d\Omega \tag{10b}$$

is the directional weight at wall and it becomes $-D_n^{mn}$, $-D_b^{mn}$, and $-D_t^{mn}$ at side ($r = r_c$), bottom ($z = 0$), and top ($z = z_c$) walls of the cylindrical enclosure, respectively.

An iterative solution is necessary because the source term due to in-scattering and the boundary conditions depend on the radiative intensity. This iterative solution is terminated when the following convergence criterion is attained:

$$\max\left(\left|I_P^{mn} - I_P^{mn,\text{old}}\right|/I_P^{mn}\right) \leqslant 10^{-6} \tag{11}$$

where $I_P^{mn,\text{old}}$ is the previous iteration value of $I_P^{mn}$. Once the intensity field is obtained, the radiative heat flux in the radial and axial directions can be estimated by

$$q_r^R = 2\sum_{m=1}^{N_\theta}\sum_{n=1}^{N_\phi} I^{mn} D_n^{mn} \tag{12a}$$

$$q_z^R = 2\sum_{m=1}^{N_\theta}\sum_{n=1}^{N_\phi} I^{mn} D_t^{mn} \tag{12b}$$

This completes the finite volume formulations for the calculation of radiative heat transfer in the axisymmetric enclosure.

### 2.3. Solution procedure

The solution procedure is straightforward because the final discretization equation in Eq. (9) is the spatial two-dimensional form, which is commonly used in the CFD with combustion and heat transfer. All the points in the calculation domain are swept along the direction of radiation propagation. There exist four sweep directions according to the directional weights $D_n^{mn}$ and $D_t^{mn}$. For example, when $D_n^{mn} > 0$ and $D_t^{mn} > 0$, the sweep proceeds from centerline ($r = 0$) to outer boundary ($r = r_c$) and bottom ($z = 0$) to top boundaries ($z = z_c$). This procedure is common in the DOM [2,3,10] and the FVM [8,13,14].

Another point of view of the solution procedure is the three-dimensional form followed by Chui et al. [5], in which axisymmetric intensity is transformed into $I(r, \varphi_0, z, \theta, \varphi_\Omega = 0)$, i.e., spatial three-dimensional and angular one-dimensional systems. To explain this procedure it is helpful to revisit Fig. 2. As explained before, the intensities in Fig. 2b completely describe the axisymmetric intensity field shown in Fig. 2a. To apply this procedure to the present method, the intensity in Eq. (9d) $I_P^{mn-1}$ is changed to $I_W^{mn-1}$ (i.e. west control volume intensity) without any other modification. Then, above mentioned three-dimensional procedure can be directly used. Consider an arbitrary constant $z$-plane as shown in Fig. 2b. For $\pi > \varphi_0 > \pi/2$, i.e. $I_2^1$ and $I_3^1$ in the left side quadrant in Fig. 2b, because the intensity is influenced by that of the upstream face, the solution is marched from the outer cylindrical wall to the inner center point $O$. Similarly for $\pi/2 > \varphi_0 > 0$, i.e. $I_4^1$ and $I_5^1$ in the right side quadrant in Fig. 2b, the calculation procedure is marched from the inner center point $O$ to the outer cylindrical wall. Along the horizontal face ($y = 0$ line) no intensity at the boundary face is required since $D_w^{m2-1/2} = 0$ and $D_e^{mN_\phi+1/2} = 0$ as illustrated in Fig. 5. Strictly speaking, this face is a symmetry face, therefore, physically

no heat can transport across this surface. This marching procedure is repeated in any axial $z$-plane from bottom to top walls when $D_t^{mn} > 0$ or from top to bottom walls when $D_t^{mn} < 0$. Here, it is noticed that the present solution procedure is similar to that of Chui et al. [5] in view of spatial three-dimensional calculation for axisymmetric intensity although the present solution method is formulated using the cylindrical base vectors for both spatial and angular coordinates rather than Cartesian base vectors adopted by Chui et al. [5].

### 2.4. Comparison with other solution methods

Recently, various forms of the finite volume and discrete ordinates formulations for the analysis of axisymmetric radiative heat transfer are suggested by considering the geometric and directional characteristics of the axisymmetric coordinate. These methods can be summarized as two categories according to the choice of the angular base vectors, Cartesian [5–7,13] or cylindrical [8,14] ones, because, as discussed by Moder et al. [6], the occurrence of angular redistribution terms is determined by which angular coordinates are held fixed during the volume integral of streaming term, d$I$/d$s$, represented in the LHS of Eq. (2). The Cartesian angular coordinate employs $(\theta,\varphi_\Omega)$ system which has a fixed direction $\vec{s} = \vec{e}_x \sin\theta\cos\varphi_\Omega + \vec{e}_y \sin\theta\sin\varphi_\Omega + \vec{e}_z\cos\theta$ in $(\theta,\varphi_\Omega)$ coordinates regardless of spatial $\varphi_0$ location, therefore, angular redistribution terms will not occur for the DOM and FVM. The cylindrical angular coordinate, however, adopts $(\theta,\phi)$ system such that angular direction $\vec{s} = \vec{e}_r \sin\theta\cos\phi + \vec{e}_{\varphi_0}\sin\theta\sin\phi + \vec{e}_z\cos\theta$ varies with the spatial $\varphi_0$ location and, therefore, angular redistribution terms will occur for DOM and FVM.

From this point of view, the two- or three-dimensional procedure adopted in this work can be seen as an alternative form of the works by Murthy and Mathur [8], Tian and Chiu [13], and Ben Salah et al. [14] in case of spatial two-dimensional work, and Chui et al. [5], Moder et al. [6], and Kim and Baek [7] for three-dimensional procedure.

Attention is now turned to the modeling of the redistribution terms caused by angular cylindrical coordinate. In the conventional [2,3] and modified DOM [10], angular derivative term is modeled using the conventional artifice [1,9], which maintains neutron conservation and permits minimal directional coupling:

$$-\frac{1}{r}\frac{\partial}{\partial\phi}(\eta I) \simeq \frac{\alpha^{mn-1/2} I_P^{mn-1/2} - \alpha^{mn+1/2} I_P^{mn+1/2}}{\Delta\Omega^{mn}} \tag{13}$$

where $\alpha^{mn\pm1/2}$ is the coefficient for the angular derivative term to be determined. Here, a recursive relation of the coefficients for the angular derivative term, $\alpha^{mn\pm1/2}$, can be determined by examining the divergenceless flow condition by Carlson and Lathrop [1] and Lewis and Miller [9] as follows:

$$\alpha^{mn+1/2} - \alpha^{mn-1/2} = 2\mu^{mn} w^{mn} = 2D_r^{mn} \tag{14}$$

with an assumption of $\alpha^{m1/2} = 0$ as a starting point. Then, this expression provides a recursive relation for determining the constants, $\alpha^{mn\pm1/2}$. Note that, since the directional weights are analogous to the multiplication of direction cosine by quadrature weight in the conventional DOM, Eq. (6) corresponds to another form of the recursive relation [1–3]. In the current procedure, however, it is not required to determine the $\alpha^{mn\pm1/2}$ terms because its finite volume forms are determined from angular and geometric considerations via angular edge directional weights. From this point of view, this work is regarded as the generalization of the practice by Ben Salah et al. [14], where analytical form of the $\alpha^{mn\pm1/2}$ term is developed by considering axisymmetric situations in the finite volume category.

## 3. Results and discussion

The solution procedures presented above is applied to axisymmetric radiative heat transfer problems of (1) enclosure with absorbing–emitting medium, (2) enclosure with anisotropically scattering medium, (3) rocket plume base heating, (4) furnace with measured data, (5) furnace with unknown medium temperature, and (6) enclosure with non-gray gas and particle mixture. For all cases presented below, $(N_r \times N_z)$ number of equally spaced control volumes are used. The total solid angle $2\pi$ is divided into $(N_\theta \times N_\phi)$ directions with uniform $\Delta\theta^m = \theta^{m+} - \theta^{m-} = 0.5\pi/N_\theta$ and $\Delta\phi^n = \phi^{n+1/2} - \phi^{n-1/2} = 2\pi/N_\phi$, while spatial azimuthal angle is discretized as $N_{\varphi_0} = N_\phi$ with $\Delta\varphi_0 = \Delta\phi$.

### 3.1. Enclosure with absorbing–emitting medium

Based on the present formulations, the problem of a finite cylindrical enclosure containing absorbing–emitting medium with constant temperature and absorption coefficient is demonstrated and compared with the exact solutions. The enclosure with $r_c = 1$m and $z_c = 2$m is cold ($T_w = 0$ K) and black ($\varepsilon_w = 1$), and the enclosed medium is hot as $T_g = T_{ref}$ and has three different absorption coefficients of $\kappa_a = 0.1$, 1.0, and 5.0m$^{-1}$. In this example, the exact intensity at any location within the enclosure is given by the summation of all the intensities from the enclosure wall as well as local emission of the medium such as

$$I(s) = I_{bw} e^{-\kappa_a s} + I_b(1 - e^{-\kappa_a s}) \tag{15}$$

where $I_b$ is the blackbody intensity of the homogeneous medium, and $s$ is the path length. The exact wall heat flux can be obtained by numerically integrating $I(s)(\vec{s}\cdot\vec{n}_w)$ over all incident solid angles via Gaussian quadrature numerical integration.

To check the accuracy of each algorithm, the number of control volume used is kept the same as $N_r = 17$ and $N_z = 33$, while for angular discretization three different angular grid (control angle) systems of $(N_\theta \times N_\phi) = (8 \times 6)$, $(12 \times 10)$, and $(16 \times 14)$ are applied. Fig. 6 shows the non-dimensional wall heat flux, $q^* = q_r^R/\sigma T_{ref}^4$ on the side wall for three different optical thickness of $\kappa_a = 0.1$, 1.0, and 5.0 m$^{-1}$. When the absorption coefficient is as large as $\kappa_a = 5.0$ m$^{-1}$, the radiant energy arriving on the wall approaches black body intensity of the medium $I_b = \sigma T_{ref}^4$ due to heat blockage effect, i.e. the thick medium absorbs nearly all the radiation from neighboring medium and the intensity impinging on the wall is influenced only by the emission of the hot gas near the enclosing wall. Near the corner, however, a sharp decrease in radiant heat flux is observed because of the effect of neighboring cold top and bottom walls. But when absorption coefficient is as small as $\kappa_a = 0.1$ m$^{-1}$, the emission of the medium is weak, and the radiant heat flux is significantly reduced. This is due to the far-reaching effect of the other cold walls and negligible self-extinction of the optically thin gas.

Overall, the present solution is found to be accurate compared with the exact solution. The maximum error between the present and exact solution is 3.8% at $\kappa_a = 1.0$ m$^{-1}$ case with $(N_\theta \times N_\phi) = (8 \times 6)$. As the angular grid systems are denser to $(N_\theta \times N_\phi) = (16 \times 14)$ the maximum error reduces to 1.9%. The computation time required for the calculations shown in Fig. 6 is within 2 s using a 1.7 MHz personal computer.

### 3.2. Enclosure with anisotropically scattering medium

The second benchmark case considers a hot side ($E_{bw} = 1$) wall exposed to diffuse incident radiation in a cold medium. All walls are black ($\varepsilon_w = 1$). The cylinder has a height of $z_c = 2$m and a radius of $r_c = 1$ m. The medium has an extinction coefficient $\beta = 1.0$ m$^{-1}$ and single scattering albedo $\omega_0 = 1.0$. For the case of anisotropic

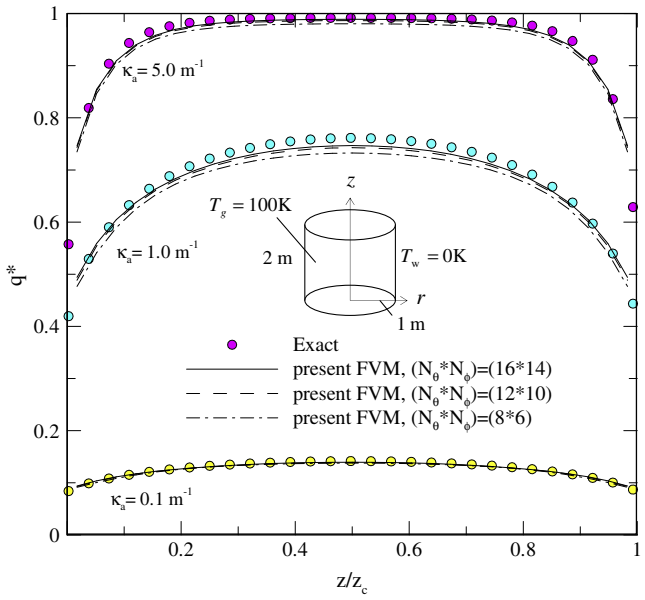


**Fig. 6.** Comparison of non-dimensional radial heat flux distribution on the side wall for three absorption coefficients for the problem of absorbing and emitting medium. The used grid systems are $(N_r \times N_z) = (17 \times 33)$ and $(N_\theta \times N_\phi) = (8 \times 6)$, (12 - 10), and $(16 \times 14)$.

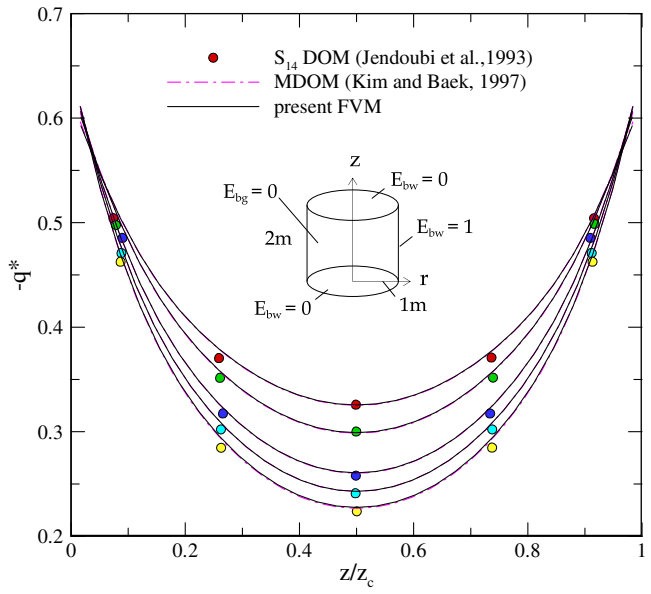


**Fig. 7.** The effect of scattering phase function on the radial radiative heat flux distribution for the problem of side wall diffuse incidence with absorbing and scattering medium. The grid systems used are $(N_r \times N_z) = (13 \times 29)$ and $(N_\theta \times N_\phi) = (12 \times 12)$.

scattering, the scattering phase function is approximated by a finite series of Legendre polynomials as follows:

$$\Phi^{m'n' \to mn} = \Phi(\cos\Psi) = \sum_{j=0}^{J} C_j P_j(\cos\Psi) \tag{16}$$

where $\Psi$ is the scattering angle between incoming direction $\vec{s}'$ and outgoing direction $\vec{s}$. $C_j$'s are the expansion coefficients. The forward (F2,F3) and backward (B1,B2) scattering phase function as given by Kim and Lee [15] are considered in addition to isotropic scattering ($\Phi = 1$). The asymmetry factors in the phase function for the case of F2, F3, isotropic, B1 and B2 are 0.670, 0.40, 0.0, −0.188 and −0.40, respectively [15]. The computational grid used has dimensions of $(N_r \times N_z) = (13 \times 29)$ and $(N_\theta \times N_\phi) = (12 \times 12)$.

Variations of the dimensionless radial radiative heat flux on the side wall are shown in Fig. 7 for all five phase functions considered in this study and compared with the works of Jendoubi et al. [16] and Baek and Kim [10], where $S_{14}$ DOM and modified DOM are used, respectively. Fig. 7 shows that the forward-scattering phase functions give larger heat fluxes than the backward-scattering phase functions from the side wall to the medium since the backward scattering distributes more radiant energy to the hot side wall. As shown in Fig. 7 the present results are in good agreement with the $S_{14}$ DOM and MDOM and, especially, the present FVM and MDOM give nearly the same results.

### 3.3. Rocket plume base heating

The third benchmark case examines an analysis of radiative base heating by the rocket exhaust plume. This problem has attracted a considerable attention during the past few decades, since the base plane should be protected against the radiative heating by the exhaust plume. Its schematic is shown in Fig. 8. The cylindrical exhaust plume with $Z_{pl} = 10R_{ex}$ is assumed to be cold ($T_g = 0$ K) and purely scatters ($\omega_0 = 1$ and $\tau_0 = \sigma_s R_{ex}$) the radiant energy emerging from the nozzle exit maintained at $T_{ref}$. The environment is considered to be cold and non-participating ($\omega_0 = \tau_0 = 0$). This situation illustrates a so-called searchlight emission, since the radiation photons emitted only from the inside of the rocket nozzle is scattered

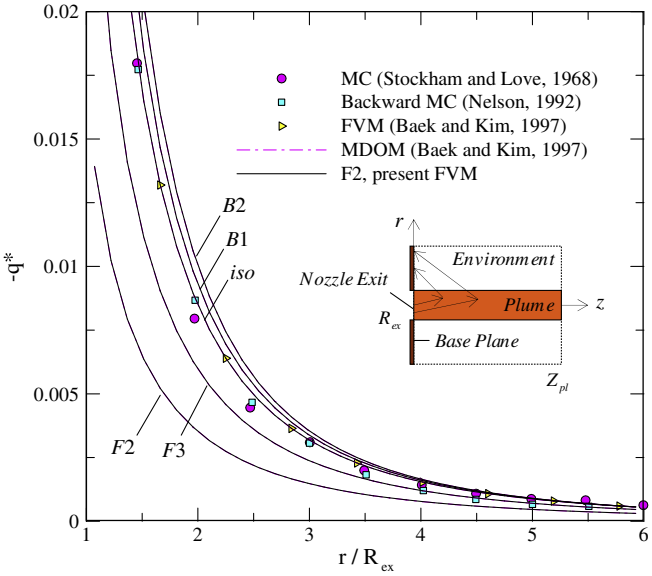


**Fig. 8.** The effect of scattering phase function on the base heating due to searchlight emission. The cold exhaust plume with $Z_{pl}/R_{ex} = 10$ has $\omega = 1$ and $\tau = 0.5$, while the cold environment does not participate radiation ($\omega = 0$ and $\tau = 0$). The number of grids used is $(N_r \times N_z) = (38 \times 48)$ and $(N_\theta \times N_\phi) = (10 \times 8)$.

by the exhaust plume towards the base plane [10,12,17,18]. The computational domain is taken a $r_c/R_{ex} = 6$ in radius and $z_c = Z_{pl} = 10R_{ex}$ in height. The number of grids used is $(N_r \times N_z) \times (N_\theta \times N_\phi) = (38 \times 48) \times (10 \times 8)$. For the case of anisotropic scattering, anisotropic scattering phase function in Eq. (17) is used.

Fig. 8 shows the effect of scattering phase function on the radiative heating, $-q^* = -q_z^R/\sigma T_{ref}^4$ on the base plane at $z = 0$. The radiative heat flux on the base plane is seen to rapidly decrease as $r/R_{ex}$ increases because the base plane views a smaller portion of the exhaust plume. In other words, the view factor toward the exhaust plume seen by a thin annulus of radius $r$ on the base plane decreases with increasing $r$. For the case of isotropic scattering

($\Phi = 1$), the present FVM solutions are in good agreement with other solutions by the Monte Carlo [17], backward Monte Carlo [18], FVM [12], and MDOM [10]. The effect of anisotropic scattering on the base heating is also shown in Fig. 8. The backward scattering (B1, B2) is observed to enhance the base heating than the forward scattering (F2, F3). This is because the photons emitted from the rocket nozzle are more scattered in the backward direction. It is noted that the present FVM works very well even when participating (plume) and non-participating (environment) media coexist.

### 3.4. Furnace with measured data

The FVM is then applied to a problem of non-swirling natural gas flame in International Flame Research Foundation test furnace [19]. A water-cooled cylindrical furnace has $r_c = 0.45$ m in radius and $Z_c = 5.0$ m in length. The wall temperature and emissivity are $T_w = 425$ K and $\varepsilon_w = 0.8$, while the blackbody inlet (left) and exit (right) temperatures are 425 K and 300 K, respectively. Measured temperatures for non-scattering gray medium with absorption coefficient of $\kappa_a = 0.3\ \mathrm{m}^{-1}$ are listed in Jamaluddin and Smith [3] following the work of Wu and Fricker [19].

Many researchers have attempted to model this furnace problem in order to validate their radiation solution methods, since well-defined experimental data are available. In Fig. 9 the present solution for the net radial heat flux on the furnace side wall is compared with other solutions obtained by $P_3$ approximations [20], conventional $S_4$ DOM [3], FVM [5], and MDOM [10] as well as the experimental data [19]. Our prediction produces similar results obtained by the others in the distribution of radial heat flux. It must be noted that the present prediction yields nearly similar solution by the FVM [12] and MDOM [10] with a similar grid system of $(N_r \times N_z) = (3 \times 17)$ and $(N_\theta \times N_\phi) = (8 \times 12)$, although we have used the step scheme for spatial and angular differencing, whereas Chui et al. [5] used the exponential scheme which is computationally expensive and somewhat more complex.

### 3.5. Furnace with unknown medium temperature

For many engineering applications, there may exist non-radiative volumetric heat source, $S_{nr}$, in the medium rather than the medium temperature is given. In this case the divergence of radiative heat flux, which represents a net loss of radiant energy from a control volume, has to be equal to this source satisfying the following equation for energy conservation [21]:

$$S_{nr} = \nabla \cdot q^R = \kappa_a \left( 4\pi I_b - \int_{\Omega=4\pi} I \, d\Omega \right) \tag{17}$$

The blackbody intensity obtained from the above equation is inserted into Eq. (5b) and, thereby, the intensity field could be calculated. It is noted that when the medium is in radiative equilibrium, i.e., $S_{nr} = 0$, temperature distribution of the medium can be obtained directly from $4\pi I_b = \int_{\Omega=4\pi} I \, d\Omega$.

The test furnace has the radius of $r_c = 1$ m and the length of $z_c = 4$ m. The physical conditions are $T_w = 1200$ K, $\varepsilon_w = 0.85$ for bottom wall ($z = 0$), 400 K and 0.7 for top wall ($z = Z_c$), 900 K and 0.7 for side wall ($r = r_c$). Other properties for the isotropically scattering medium are $\omega_0 = 0.7$, $S_{nr} = 5.0\ \mathrm{kW/m^3}$ and three extinction coefficients are $\beta_0 = 0.1$, 1.0, and $5.0\ \mathrm{m}^{-1}$. Fig. 10 illustrates a comparison of the medium temperature at $z = 2.0$ m for different optical thicknesses. As the extinction coefficient decreases from 5.0 to 0.1, the temperature of the medium becomes much higher due to the far-reaching effect of the hot wall. Therefore, the medium temperature becomes more uniform, whereas the temperature gradient at the side wall is steeper for the case of smaller optical thickness. In the above, the present solutions are compared with the results by the modified discrete ordinates solutions [10]. It is noted that the two solutions are almost identical. In these calculations, the same grid system of $(N_r \times N_z) = (12 \times 24)$ and $(N_\theta \times N_\phi) = (8 \times 12)$ and the step scheme for spatial differencing are used in both FVM and MDOM.

### 3.6. Enclosure with non-gray gas and particle mixture

Finally, the present finite volume formulations are applied to the problem of axisymmetric radiative heat transfer with a two phase mixture of non-gray gas with particles, which often occurs in the combustion systems including soot particles and non-gray combustion products such as $H_2O$ and $CO_2$. To model such situa-

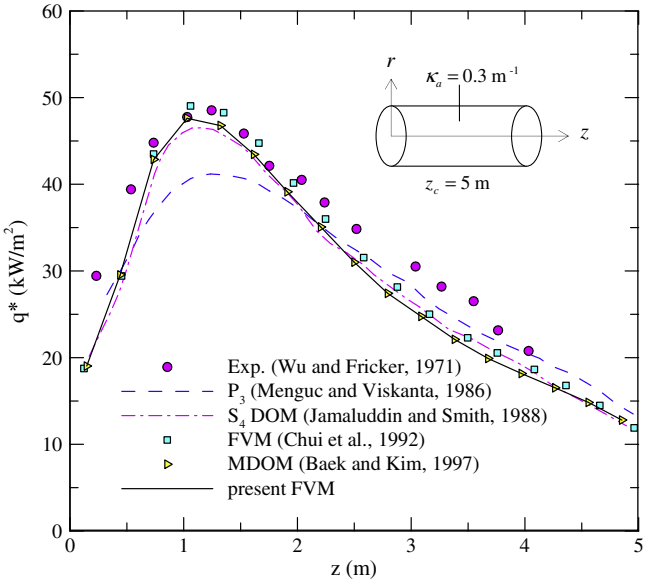


**Fig. 9.** Comparison of radial heat flux at the side wall with the experimental and other predictions. Spatial $(N_r \times N_z) = (3 \times 17)$ and angular $(N_\theta \times N_\phi) = (8 \times 12)$ systems are used.

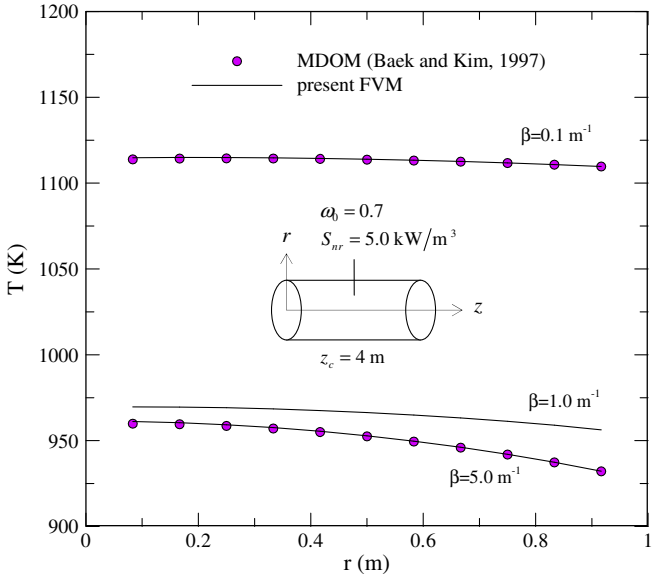


**Fig. 10.** Comparison of the medium temperature at $z = 2$ m for three different extinction coefficients of $\beta = 0.1$, 1.0, and $5.0\ \mathrm{m}^{-1}$. The medium has $\omega_0 = 0.7$ and volumetric non-radiative heat source of $S_{nr} = 5.0\ \mathrm{kW/m^3}$. The spatial and angular mesh systems of $(N_r \times N_z) = (12 \times 24)$ and $(N_\theta \times N_\phi) = (8 \times 12)$ are adopted.

tions with the present approach, some modifications for the governing RTE are required such that

$$\frac{dI_k}{ds} = -\beta_k I_k + w_{g,k}(T_g)\kappa_{g,k} I_{b,g} + w_{p,k}(T_p)\kappa_p I_{b,p} + \frac{\sigma_{sp}}{4\pi}\int_{\Omega'=4\pi} I_k(\vec{s}')\Phi(\vec{s}',\vec{s})d\Omega' \quad (18)$$

where $I_k$, $I_{b,g}$, and $I_{b,p}$ are the $k$th band radiative intensity, blackbody intensity of gas and particles, respectively. $\beta_k = \kappa_{g,k} + \kappa_p + \sigma_{sp}$ is the extinction coefficient, where $\kappa_{g,k}$ is the $k$th band absorption coefficient of mixture gases, $\kappa_p$ and $\sigma_{sp}$ are the absorption and scattering coefficients of particles, respectively. In addition, $w_{g,k}(T_g)$ and $w_{p,k}(T_p)$ are the weighting factor related to the $k$th gray band and are functions of gas temperature, $T_g$, and particle temperature, $T_p$, respectively. As suggested and validated by Yu et al. [22], if the two phase mixture of non-gray gases and particles is not in thermal equilibrium, and if the gas and particles share all the same $k$th gray bands, the weighting factor for particles has the same type as that for the gas so that $w_{p,k}(T_p) = w_{g,k}(T_p)$. Therefore, for the analysis of radiative heat transfer by mixtures of non-gray gas and particle, Eq. (9) is also used by simply changing the extinction coefficient and source terms due to non-gray gas and particles. To obtain the non-gray gas absorption coefficients and the associated weighting factors for gas and particles, the weighted sum of gray gases model (WSGGM) of Smith et al. [23] is used. The particle absorption and scattering, however, are assumed gray and obtained from Yu et al. [22] and Chui et al. [11] such as

$$\kappa_p = \varepsilon_p \sum_i N_i \frac{\pi d_i^2}{4} \quad (19a)$$

$$\sigma_{sp} = (1-\varepsilon_p) \sum_i N_i \frac{\pi d_i^2}{4} \quad (19b)$$

where $\varepsilon_p$ is the particle emissivity, $N_i$ and $\pi d_i^2/4$ are the number density and the projected area, respectively, of the particle pertaining to group $i$. More detailed discussions about the non-gray gas and particle models used here can be found in Yu et al. [22].

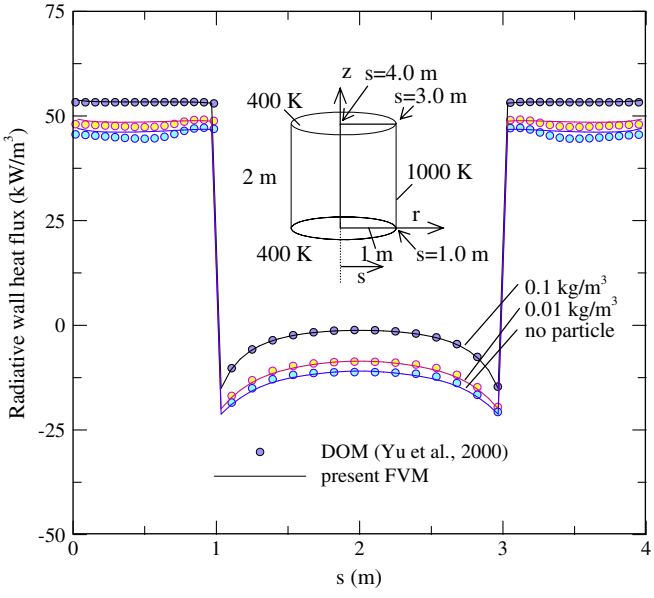


**Fig. 11.** Comparison of radiative wall heat flux along the walls of a cylindrical enclosure. All walls except side walls are black, while the medium of $T_g$ = 1000 K has 20% $H_2O$, 10% $CO_2$, and 70% transparent gas with particles of $T_p = T_g$. Scattering is isotropic. The number of grid systems used are $(N_r \times N_z) = (15 \times 30)$ and $(N_\theta \times N_\phi) = (12 \times 8)$.

To validate the present formulations, an axisymmetric enclosure with a two-phase mixture of gas and particle is considered following the work of Yu et al. [22]. A cylindrical enclosure with 1 m in radius and 2 m in length has 20% $H_2O$, 10% $CO_2$ mixture and particles. The medium has either no particles or concentration of 0.01 and 0.1 kg/m$^3$, respectively. The black top and bottom walls are kept cold at 400 K, while the side wall temperature and emissivity are 1000 K and 0.8. The scattering coefficient $\sigma_{sp}$ is a function of particle size, number density, and emissivity as in Eq. (4), while particle scattering which depends on the size and refractive index of scattering particle and scattering angle is assumed isotropic. In this work, it is assumed that the particle size is ranged in 50, 60, 70, 80, and 100 μm with 20% each by mass. Also, the particle density is taken as 1300 kg/m$^3$ with emissivity of 0.8 [22]. Therefore, in case of $C_p$ = 0.01kg/m$^3$, $\sigma_{sp}$ becomes 0.037 m$^{-1}$. The gas and particle temperatures are the same at $T_g = T_p$ = 1000 K. The grid system used in this example is $(N_r \times N_z) = (15 \times 30)$ and $(N_\theta \times N_\phi) = (12 \times 8)$. Fig. 11 shows the effect of particle concentration on radiative wall heat flux. It is found that the present solutions are in good agreement with those of Yu et al. [22].

## 4. Conclusions

A finite volume method has been proposed to analyze the radiative heat transfer in an axisymmetric cylindrical geometry with an absorbing, emitting, and scattering medium. Its discretized form of equation and solution procedure are presented. Different from the original FVM, the main feature of the present method is the choice of spatial and angular base vectors, i.e., Cartesian or cylindrical one. In order to validate the present formulation, six test problems are considered and their solutions are compared with exact or other predictions. All the results presented in this work show that the present method is accurate and valuable for the analysis of axisymmetric radiative heat transfer problems with radiatively active medium including gray, non-gray and particle mixture.

## Acknowledgement

This work is supported by the Research Center of Industrial Technology at Chonbuk National University, Korea.

## References

[1] B.G. Carlson, K.D. Lathrop, Transport theory – the method of discrete ordinates, in: H. Greenspan, C.N. Kelber, D. Okrent (Eds.), Computing Methods in Reactor Physics, Gorden and Breach Science Publications, New York, 1968, pp. 165–266.
[2] W.A. Fiveland, A discrete-ordinates method for predicting radiative heat transfer in axisymmetric enclosure, ASME Paper 82-HT-20, 1982.
[3] A.S. Jamaluddin, P.J. Smith, Predicting radiative transfer in axisymmetric cylindrical enclosures using the discrete-ordinates method, Combust. Sci. Technol. 62 (1988) 173–186.
[4] T.Y. Kim, S.W. Baek, Thermal development of radiatively active pipe flow with nonaxisymmetric circumferential convective heat loss, Int. J. Heat Mass Transfer 39 (1996) 2969–2976.
[5] E.H. Chui, G.D. Raithby, P.M.J. Hughes, Prediction of radiative transfer in cylindrical enclosures with the finite volume method, J. Thermophys. Heat Transfer 6 (1992) 605–611.
[6] J.P. Moder, J.C. Chai, G. Parthasarathy, H.S. Lee, S.V. Patankar, Nonaxisymmetric radiative transfer in cylindrical enclosures, Numer. Heat Transfer B 30 (1996) 437–452.
[7] M.Y. Kim, S.W. Baek, Analysis of radiative transfer in cylindrical enclosures using the finite volume method, J. Thermophys. Heat Transfer 11 (1997) 246–252.
[8] J.Y. Murthy, S.R. Mathur, Radiative heat transfer in axisymmetric geometries using an unstructured finite-volume method, Numer. Heat Transfer B 33 (1998) 397–416.
[9] E.E. Lewis, W.F. Miller Jr., Computational methods of neutron transport, John Wiley and Sons, New York, 1984. pp. 135–145.
[10] S.W. Baek, M.Y. Kim, Modification of the discrete-ordinates method in an axisymmetric cylindrical geometry, Numer. Heat Transfer B 31 (1997) 313–326.

[11] E.H. Chui, P.M.J. Hughes, G.D. Raithby, Implementation of the finite volume method for calculating radiative transfer in a pulverized fuel flame, Combust. Sci. Technol. 92 (1993) 225–242.
[12] S.W. Baek, M.Y. Kim, Analysis of radiative heating of rocket plume base with the finite-volume method, Int. J. Heat Mass Transfer 40 (1997) 1501–1508.
[13] W.T. Tian, K.S. Chiu, A two-dimensional scheme for axisymmetric radiative heat transfer using the finite-volume method, Numer. Heat Transfer B 47 (2005) 199–211.
[14] M. Ben Salah, F. Askri, K. Slimi, S. Ben Nasrallah, Numerical resolution of the radiative transfer equation in a cylindrical enclosure with the finite-volume method, Int. J. Heat Mass Transfer 47 (2004) 2501–2509.
[15] T.K. Kim, H.S. Lee, Radiative heat transfer in two-dimensional anisotropic scattering media with collimated incidence, J. Quant. Spectrosc. Radiat. Transfer 42 (1989) 225–238.
[16] S. Jendoubi, H.S. Lee, T.K. Kim, Discrete-ordinates solutions for radiatively participating media in a cylindrical enclosure, J. Thermophys. Heat Transfer 7 (1993) 213–219.
[17] L.W. Stockham, T.J. Love, Radiative heat transfer from a cylindrical cloud of particles, AIAA J. 6 (1968) 1935–1940.
[18] H.F. Nelson, Backward Monte Carlo modeling for rocket plume base heating, J. Thermophys. Heat Transfer 6 (1992) 556–558.
[19] H.L. Wu, N. Fricker, An investigation of the behavior of swirling jet flames in a narrow cylindrical furnace, in: Second Members' Conference, International Flame Research Foundation, IJmuiden, The Netherlands, 1971.
[20] M.P. Menguc, R. Viskanta, Radiative transfer in axisymmetric, finite cylindrical enclosures, J. Heat Transfer 108 (1986) 271–276.
[21] M.F. Modest, Radiative Heat Transfer, second ed., Academic Press, New York, 2003.
[22] M.J. Yu, S.W. Baek, J.H. Park, An extension of the weighted sum of fray gases non-gray gas radiation model to a two phase mixture of non-gray gas with particles, Int. J. Heat Mass Transfer 43 (2000) 1699–1713.
[23] T.F. Smith, Z.F. Shen, J.N. Friedman, Evaluation of coefficients for the weighted sum of gray gases model, J. Heat Transfer 104 (1982) 602–608.